

Paradigm Shift in Studying Joint Micro-Roughness Coefficients using Graph Theory

Mohammad Lotfi^{a, *}, Behzad Tokhmechi^a

^a Faculty of Mining, Petroleum and Geophysics Engineering, Shahrood University of Technology, Shahrood, Iran

Article History:

Received: 18 October 2018,

Revised: 13 March 2019

Accepted: 24 March 2019.

ABSTRACT

In this paper, the ranking of joint roughness coefficients (JRC) profiles is investigated as a well-known acceptable pattern for studying rough surfaces. For this purpose, the dimension of digitized profiles was measured using fractal-wavelet based methods. Digitization of these profiles and detection of asperities were carried out from a distance of 0.02 mm. The integration of results obtained from various data fusion methods including Clone-proof Schwartz Sequential Dropping (CSSD) and graph theory with that of the scientific phenomenology shows that the current trend of roughness profiles needs to be corrected. In fact, some of the exemplar profiles, unlike their appearance, have different roughness values than others. This approach changes awareness about roughness as a challenging parameter. Therefore, the robust answer was obtained with a logical inspect of data fusion and presenting a new ranking for JRC profiles (JRC_N).

Keywords : *Asperity; Clone-proof Schwartz Sequential Dropping; Data Fusion; Fractal-Wavelet based Methods; JRC*

1. Introduction

“Roughness” is one of the most challenging parameters of fractures’ surface texture. This parameter is defined as the heterogeneity with the small wavelength and high frequency that we want to measure it. This deviation, which is interpreted as the wavelength with frequency, is measured relative to the smooth surface that is completely flat (Hudson and Harrison 1997). Roughness, in addition to the stress regime, depends on rock type and mineralogy. For example, Basalt, Gneiss, Quartzite, Granite, and Marble have different roughness values (McWilliams *et al.* 1993; Moosavi *et al.* 2013). This parameter is hardly studied due to its specific structural nature. Hence, numerous studies have been conducted on this parameter. One the most well-known patterns in this case is Joint Roughness Coefficients (JRC). Based on this pattern, ten profiles with increasing roughness have been presented (Barton 1973; Barton and Choubey 1977) and accepted by the researchers. However, many improvements and modifications have already been made on these exemplar profiles (Ghazvinian and Mohebi 2012; Tatone and Grasselli 2013; Amanloo and Hosseinitoudeshki 2013; Yong *et al.* 2018).

There are many methods for studying rough surfaces including mechanical methods (Halling 1976; ASME, 1978; Thomas 1982; Develi 1996), optical methods (Olsen and Adams 1970; Hung Yau 1978; Huang *et al.* 2016), Similarity-based methods (Wu and Mendel 2008; Ye 2011, 2012; Broumi and Smarandache 2013; Majumdar and Samanta 2014; Ye 2014, 2015) and computational methods (Brigham 1974; Barton and La Pointe 1995; Thachaparambil 2015). Some of the computational methods are based on Hausdorff’s Theorem. In Hausdorff-based method, the volume of coverings is considered by rectangles. Then, they are popularized to the desired metric spaces (Shah 2009). In this regard, Orey (1970) studied the gaussian sample functions and the dimension of level crossing based on Hausdorff’s Theorem. Tatone (2009)

quantitatively characterized natural rock discontinuity roughness in-situ and in the laboratory. For this purpose, he digitized JRC profiles with a horizontal point spacing of 0.50 mm. Then, he analyzed 2D profiles using the 3D roughness evaluation methodology. Also, Tatone and Grasselli (2010) presented a regression equation for JRC-based on digitized profiles from a distance of 0.50 mm and 1.00 mm.

The other part of the computational methods is based on wavelet transform and their number is based on the fractal geometry. These methods, due to their computational structure, will present accurate results. For example, Lee *et al.* (1998) applied the wavelet transform for characterization of engineered surfaces. Two years later, Josso (2000) presented space-frequency analytical methods based on wavelet analysis in his PhD dissertation and applied his strategy for characterization of rough surfaces (Josso *et al.* 2001). Also, he used a frequency normalized wavelet transform (FNWT) method for surface roughness analysis and characterization (Josso *et al.* 2002). Arizabalo *et al.* (2004) estimated Hurst’s coefficient and fractal dimension from well log data using wavelet analysis. Grzeski and Brol (2009) characterized rough surfaces using wavelet transform and fractal geometry. Morala-Argüello *et al.* (2012) evaluated surface roughness classes applying haar wavelet. In all methods that are based on the wavelet transform, the roughness profile is considered as a signal, and the accommodation of the local wavelet is measured with the signal.

Rocks, due to their internal structure and heterogeneous, appear in the format of fractal geometry in the simulation process (Tzschichholz and Herrmann 1995). This issue has also been studied by many researchers (Brown 1987; Dubuc *et al.* 1989; Miller *et al.* 1990; Huang *et al.* 1992; Den Outer *et al.* 1995; Xie *et al.* 1997; Glover *et al.* 1999; Babadagli and Develi 2001; Murata *et al.* 2002; Seno 2003; Cerepi 2004; Tran and Tran 2007; Zhang *et al.* 2014; Du *et al.* 2015; Suleimanov *et al.* 2017; Zuo *et al.* 2017). Among the methods that are based on fractal geometry, the common methods include box-counting, power spectral analysis, geostatistical method, and divider (Cox and Wang 1993;

* Corresponding author. E-mail address: mohammad.lotfi@shahroodut.ac.ir (M. Lotfi).

Carpinteri and Chiaia 1995; Seidel and Haberfeld 1995; Chun and Kim 2001). In the box-counting method, roughness profile survey by small-size squares as boxes. These boxes cover the whole profile and counted. Finally, the dimension is obtained by calculating the number of the variation of boxes versus the size of each box. This process is repeated until the box size approaches zero (Feder 1988; Kulatilake *et al.* 1995). Um (1997) developed a new peak shear strength criterion for joints using the box-counting method. Nayak and Mishra (2016) estimated the fractal dimension of the roughness of color images using an improved differential box-counting method and its application on 24-bit images. Panigrahy *et al.* (2017) estimated the fractal dimensions of gray-scale images using the differential-box-counting method. Spectral analysis is a method that can be considered as the fast Fourier transform (FFT) analysis. In fact, desired results can be obtained using FFT in 1D and 2D (Saupe 1988; Press *et al.* 1992; Roko *et al.* 1997). Chae *et al.* (2004) measured the roughness of rock discontinuities using a confocal laser scanning microscope and the FFT. Osterloo *et al.* (2012) studied the effect of roughness on the thermal infrared spectra of rock surfaces. Jain and Pitchumani (2017) worked on a fractal model for wettability of rough surfaces using this method. Geostatistical methods as spatial analytical approaches are used for measuring roughness by using the variogram model (Ferrero *et al.* 1999). For example, Kulatilake *et al.* (1998) investigated the requirements for accurate quantification of self-affine roughness using the variogram method. Arizabalo *et al.* (2004) analyzed a naturally fractured limestone reservoir in the Gulf of Mexico using this method. Also, Rasouli and Tokhmechi (2010) applied this method on the reservoir simulation and estimation of porosity. Mooney and Boisvert (2015) populated veins and modeled the grade in a coarse gold deposit using the variogram model. In the divider method, desired profiles are scrolled by a divider with a variable size. These sizes change in each iteration. Finally, the dimension is obtained by plotting the change of a number of iteration multiplied by the size of divider versus the size of the divider in a full logarithmic scale (Lee *et al.* 1990). Maerz *et al.* (1990) measured the roughness of joints using the shadow profilometry based on the divider method. Profilometry is a suitable method for 2D measuring based on which some scanners are designed (Unal 2000). Shou (1994) investigated the effect of roughness on the peak shear strength of joints applying. Bae *et al.* (2011) added the remaining amount to the measurements and calculated the fractal dimension with new parameters. Li and Huang (2015) developed this method and suggested a new equation for measuring the dimension.

In the case of JRC profiles, as the number increases roughness is obviously expected to increase as well; in reality, however, by using any of the common methods, this phenomenon does not actually occur. Regardless of the difference in the results that return to the methodology, the decision in this field can be controversial. To reduce ambiguity and increase assurance, data fusion methods are used at the decision level. For this purpose, all joint roughness coefficient exemplar profiles are digitized with high accuracy. Therefore, we digitized the profiles for all of them with an average of 5500 data for each profile. Then, fractal- and wavelet-based methods were applied for measuring the fractal dimension. Also, Clone-proof Schwartz Sequential Dropping

(CSSD) and Borda Count (BC) were applied on obtained results for decision making, while reducing ambiguity and presenting a robust answer.

2. Digitizing Process

Generally, roughness can be studied at two macro-roughness and micro-roughness levels. As seen in Figure 1, macro-roughness that is also called waviness has a global trend; while micro-roughness as unevenness has a local trend. For detecting this detail, multiple profiles have been studied on a micro scale as Joint Micro-Roughness Coefficients. In this regard, Tse and Cruden (1979) digitized the JRC profiles at an interval of 1.27 mm. Yu and Vayssade (1991) digitized them at intervals 0.25 mm, 0.50 mm, and 1.00 mm. Yang *et al.* (2001) digitized JRC with a distance of 0.50 mm and presented a regression equation for them. Tatone and Grasselli (2010) also digitized them at intervals 0.50 mm and 1.00 mm. Yong *et al.* (2018) digitized standard roughness profiles under different sampling intervals 0.10 cm and 0.50 cm.

According to the approach, the search space for analysis of rough exemplar profiles will be equivalent to their length. In other words, the search space along the “x” axis represents the length of the profile in this direction. The space corresponding to each of the digitized points along the “y” axis shows the roughness value. Therefore, higher roughness values correspond with more asperity along the “y” axis. The search space along the “x” axis is another important point. Regarding the exemplar profiles, two types of roughness can be considered on a micro and macro scale (Figure 1). Due to the micro-roughness (local trend) of the profiles compared with macro-roughness (global trend), detecting points on them must be accurate; because this study examines the micro-scale roughness. Therefore, this is closer to reality to decide on roughness. For this purpose, the points were taken with a resolution of 0.02 mm along with the profile. Obviously, if the distance between the points is small, the variability can be better displayed. This resolution can provide a reasonable assurance of the detection of two types of asperities. All roughness profiles were digitized with an average of 5500 data for each profile (Figure 2) through this process and all methods were applied to them.

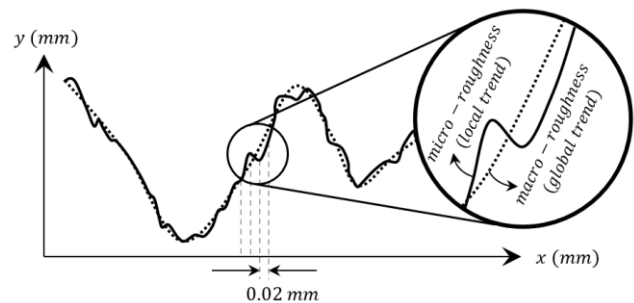


Figure 1. Point detection considering two types of roughness.

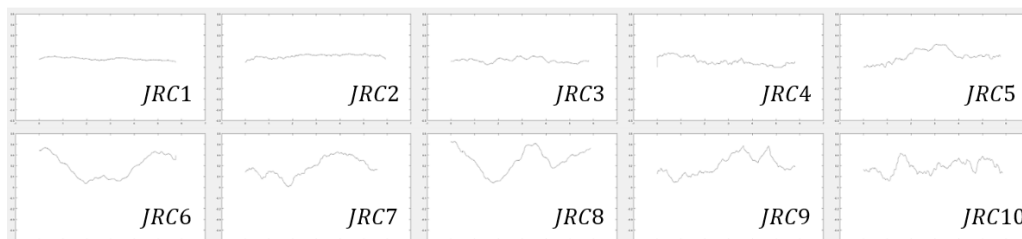


Figure 2. Digitized profiles of JRC at interval 0.02 mm. Profiles are rescaled for better display. They have been squeezed in “x” axis and have been stretched in “y” axis.

3. Methodology

In the following sections, two approaches are described for measuring the roughness of surfaces. These approaches include 5 methods. In addition, we used the results obtained from three methods based on

different approaches. The CSSD or the beat path method was applied for the integration of the results. The Borda Count data fusion method was used for decision making in the case of ambiguity on similar results. All these steps are displayed in the flowchart depicted in Figure 3. As prologue presented in Figure 3, the roughness exemplar profiles were digitized accurately (Figure 2) before using any methods.

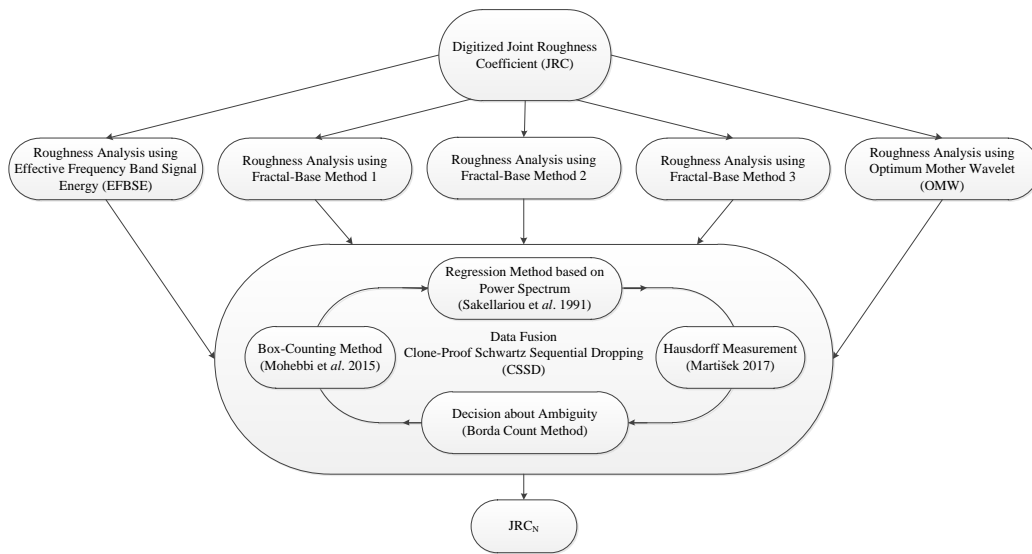


Figure 3. The flowchart of the study.

3.1. Fractal-Based Approach

The measured fractal dimension includes a topological dimension. Therefore, increasing the roughness profiles will consequently increase their fractal dimension. In method 1, the length of the profile was surveyed frequently (Figure 4). N is the frequency number. For each step of measurement, the size of divider (r) gradually increase and this size is fixed in the whole step. Plotting r versus Nr in a log-log scale, the fractal dimension is obtained from equation 1 (Maerz *et al.* 1990).

$$D = 1 - \frac{\Delta \log Nr}{\Delta \log r} \tag{1}$$

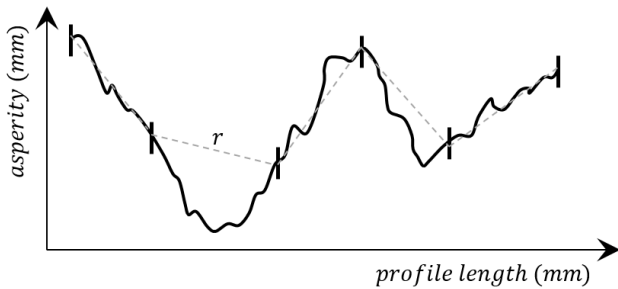


Figure 4. Schematic representation of method 1 in rescaled roughness profile surveying (Profile is rescaled for better display).

In method 2, as shown in Figure 5, the same process is conducted with this difference in which the length (f) will be added to the measurements. In other words, the fractal dimension as well as r as the size of divider and N as the number of the survey repetition depend on f . Finally, the dimension of the profile is obtained from Equation 2 (Bae *et al.* 2011). In this method, same as the previous one, r is the size of the divider, N is the number of steps and f is the remaining length of the profile in each step. Finally, the dimension can be measured through plotting $N + f/r$ versus r in a log-log scale (Figure 6).

$$-D = \frac{\Delta \log [N + \frac{f}{r}]}{\Delta \log r} \tag{2}$$

The third method (Method 3) obtains the fractal dimension through the calculation of variations r versus N in a log-log scale through the Equation 3 (Li and Huang 2015). Like the previous method, r is the size of divider and N is the step number.

$$-D = \frac{\Delta \log N}{\Delta \log r} \tag{3}$$

3.2. Wavelet-Based Approach

In the wavelet-based method as mentioned in the following equations, the continuous wavelet transform (CWT) (Equation 4) is used where λ is the scale parameter (with a positive sign), l is the transmission parameter in a limited range and u is variability (Tokhmechi *et al.* 2016). Then, the roughness exemplar profiles are analyzed (Figure 7).

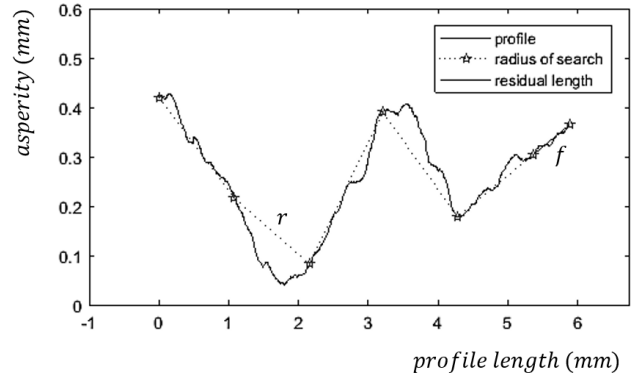


Figure 5. Application of method 2 in the JRC exemplar profile surveying (Profile was rescaled for better display).

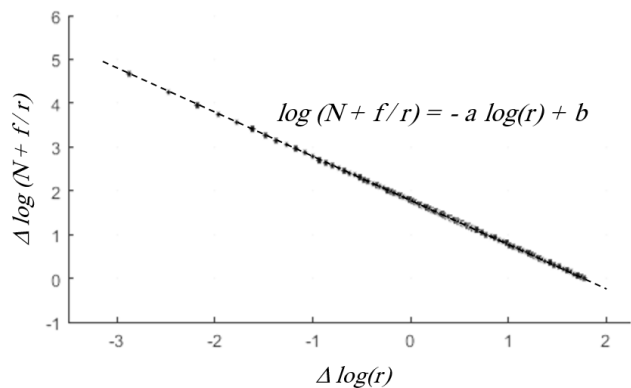


Figure 6. The general structure of plotting results in method 2 for calculating roughness.

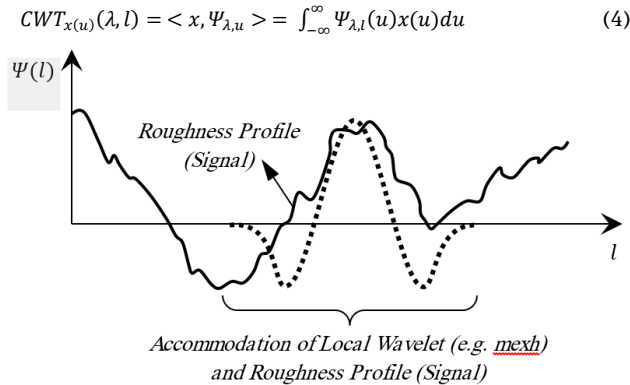


Figure 7. Accommodation between roughness profile (signal) and local wavelet (Profile is rescaled for better display).

In fact, the roughness profile is considered as the signal so that it is continuous in a period. If the signal and Fourier transform of wavelet function in the following equations (Equations 5 and 6) are true, the signal function is retrieved from Equation 7.

$$\int_{-\infty}^{\infty} x^2(l)dl < \infty \quad (5)$$

$$c_{\psi} = \int_0^{\infty} \frac{|\hat{\Psi}(f)|^2}{f} df, \quad 0 < c_{\psi} < \infty \quad (6)$$

$$x(l) = \frac{1}{c_{\psi}} \int_0^{\infty} [\int_{-\infty}^{\infty} \langle x, \Psi_{\lambda, u} \rangle \Psi_{\lambda, u}(l) du] \frac{d\lambda}{\lambda^2} \quad (7)$$

where $x(0)$ is the roughness profile or signal, $\hat{\Psi}(f)$ is the Fourier transform, $\Psi(f)$ the wavelet function, $x(l)$ is the signal function and f is frequency. This method calculates the roughness intensity of profiles.

3.3. Clone-proof Schwartz Sequential Dropping

This method is known as the beat path method and is one of innovative ways based on the graph theory in which the features overcome each other (Harary 1969; Bondy and Chvatal 1976). In fact, the features and their connections form a graph (Figure 8). In the graph theory, we have vertices and edges that can be written as $G = f(V, E)$. V is a set of vertices containing $V = \{v_1, v_2, \dots, v_n\}$ and E is set of edges that contains $E = \{e_1, e_2, \dots, e_n\}$ (Khakzad and Reniers 2015; Huai et al 2018). If the edges have weights and contain some values, these values can convert the graph into a weighted graph and due to those values, can be considered as the direction for edges. Therefore, this graph converts to a weighted directional graph (Moslehian and Payhan 2005). For example, suppose the decision matrix (DM) as follows in which f_i are features.

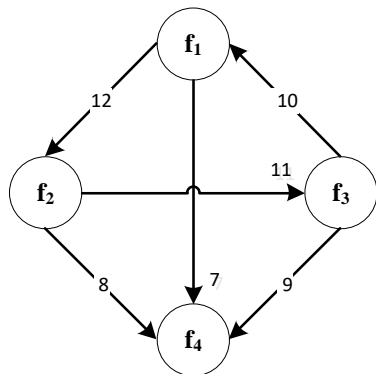
$$DM = \begin{matrix} & f_1 & f_2 & f_3 & f_4 \\ \begin{matrix} f_1 \\ f_2 \\ f_3 \\ f_4 \end{matrix} & \begin{bmatrix} - & 12 & 3 & 7 \\ 1 & - & 11 & 8 \\ 10 & 2 & - & 9 \\ 6 & 5 & 4 & - \end{bmatrix} \end{matrix}$$


Figure 8. Weighted directional graph showing paths between features.

The decision weighted directional graph for matrix DM is illustrated in Figure 8. The considered values for each edge are written according to decision matrix and a pairwise comparison must be made between the vertices. For example, the weight of edge between f_1 and f_2 based on

decision matrix from two values 12 and 1 is 12 and its direction is from f_1 to f_2 . The entire graph is drawn through the same process. The notable point is that if there is no direct edge between two vertices, one must consider the indirect path between them through the passage of other vertices. This process also must be carried out for calculating the power path of each edge. For example, the power path f_2 toward f_1 is calculated as follows: first, the path is f_2 toward f_3 whose point is 11. Second, path is f_3 toward f_1 with a point of 10. Therefore, the power path of f_2 to f_1 is equal to 10 and their connection is indirect.

3.4. Borda Count Method

In the Borda Count method, one can rate data according to their position (Fishburn 1984; Moulin 1988). This process is done in this way that if one considers all data as $M_1 = \{F_1, F_2, F_3, F_4\}$, the rate assigned to data is obtained from Equation 8.

$$Rate = (Higher\ priority) - (Lower\ priority) \quad (8)$$

In fact, the total number of times that each feature in a pairwise comparison is higher than the other features, minus the total number of times placed lower. Finally, the feature with the highest score will be selected as the preferred feature.

4. Results

In the following sections, explains the results obtained based on the fractal geometry and wavelet transform. Also, data fusion as an important part in decision making will be added separately to the results obtained from each method.

4.1. Fractal-based Analysis of JRC

In the use of fractal-based methods, we expected that increasing the number of profiles would increase roughness; however, as seen in Figure 9, the obtained results show that this process does not happen actually. A pick is seen for some JRC exemplar profiles. Therefore, after increasing roughness at these points, roughness decreases and this trend is happening again for each method separately (Table 1).

To make correct decisions about the accuracy of results with respect to the values obtained from accurate calculations, the final results of each method is ranked separately.

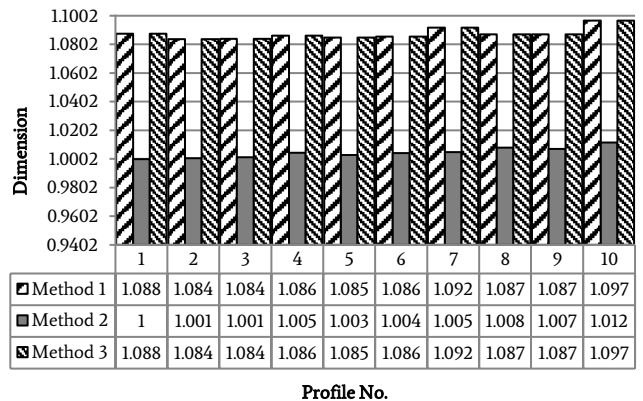


Figure 9. Obtained results based on fractal geometry for each method.

4.2. Wavelet Analysis of JRC

Through applying the wavelet transform, the Effective Signal Energy of Frequency Band (ESEFB) and Optimum Mother Wavelet (OMW) can be calculated. If JRC exemplar profiles are considered as signals, the dimension is assigned to each of the roughness profiles by applying the Fourier transform on them. These results are shown in Tables 2 and 3. These results show that despite accurate calculations of roughness, the changes in the dimension of the exemplar profiles are not incremental (Figure 10). Consequently, they are ranked to check the incremental amount of their values.

Table 1. Ranking obtained results using fractal-based methods.

Method Number	Before Ranking		After Ranking	
	Original Ranking	Fractal Dimension	Fractal Dimension	New Ranking
1	JRC ₁	1.0876	1.0838	JRC ₂
	JRC ₂	1.0838	1.0840	JRC ₃
	JRC ₃	1.0840	1.0850	JRC ₅
	JRC ₄	1.0862	1.0856	JRC ₆
	JRC ₅	1.0850	1.0862	JRC ₄
	JRC ₆	1.0856	1.0871	JRC ₈
	JRC ₇	1.0918	1.0872	JRC ₉
	JRC ₈	1.0871	1.0876	JRC ₁
	JRC ₉	1.0872	1.0918	JRC ₇
	JRC ₁₀	1.0968	1.0968	JRC ₁₀
2	JRC ₁	1.0001	1.0001	JRC ₁
	JRC ₂	1.0008	1.0008	JRC ₂
	JRC ₃	1.0014	1.0014	JRC ₃
	JRC ₄	1.0045	1.0029	JRC ₆
	JRC ₅	1.0029	1.0043	JRC ₄
	JRC ₆	1.0043	1.0045	JRC ₅
	JRC ₇	1.0050	1.0050	JRC ₇
	JRC ₈	1.0080	1.0071	JRC ₉
	JRC ₉	1.0071	1.0080	JRC ₈
	JRC ₁₀	1.0116	1.0116	JRC ₁₀
3	JRC ₁	1.0876	1.0838	JRC ₂
	JRC ₂	1.0838	1.0840	JRC ₃
	JRC ₃	1.0840	1.0850	JRC ₅
	JRC ₄	1.0862	1.0856	JRC ₆
	JRC ₅	1.0850	1.0862	JRC ₄
	JRC ₆	1.0856	1.0871	JRC ₈
	JRC ₇	1.0918	1.0872	JRC ₉
	JRC ₈	1.0871	1.0876	JRC ₁
	JRC ₉	1.0872	1.0918	JRC ₇
	JRC ₁₀	1.0968	1.0968	JRC ₁₀

Table 2. Assigned dimensions to roughness profiles after ranking the results obtained using the Effective Signal Energy of Frequency Band (ESEFB)

Original Ranking	Effective Signal Energy of Frequency Band		New Ranking	
	ESEFB (%)	Dimension	Dimension	Profile No.
JRC ₁	99.84	1.0900	1.0900	JRC ₁
JRC ₂	99.52	1.0897	1.0897	JRC ₂
JRC ₃	96.59	1.0870	1.0896	JRC ₇
JRC ₄	97.58	1.0879	1.0880	(JRC ₁₀ / JRC ₉)
JRC ₅	90.16	1.0810	1.0880	(JRC ₉ / JRC ₁₀)
JRC ₆	89.12	1.0800	1.0879	JRC ₄
JRC ₇	99.46	1.0896	1.0870	JRC ₃
JRC ₈	95.79	1.0862	1.0862	JRC ₈
JRC ₉	97.71	1.0880	1.0810	JRC ₅
JRC ₁₀	97.71	1.0880	1.0800	JRC ₆

Table 3. Assigned dimensions to roughness profiles after ranking the results obtained using the Optimum Mother Wavelet Energy (OMWE)

Original Ranking	Optimum Mother Wavelet (OMW)	Optimum Mother Wavelet Energy		New Ranking	
		OMWE (%)	Dimension	Dimension	Profile No.
JRC ₁	rbio 3.3	99.84	1.0900	1.0900	JRC ₁
JRC ₂	rbio 3.3	99.78	1.0898	1.0899	JRC ₇
JRC ₃	rbio 3.1	96.60	1.0807	1.0898	JRC ₂
JRC ₄	rbio 3.3	97.78	1.0841	1.0875	JRC ₆
JRC ₅	rbio 3.3	97.56	1.0834	1.0874	JRC ₈
JRC ₆	rbio 3.7	98.96	1.0875	1.0853	JRC ₉
JRC ₇	rbio 3.1	99.83	1.0899	1.0841	JRC ₄
JRC ₈	rbio 3.3	98.94	1.0874	1.0834	JRC ₅
JRC ₉	rbio 3.3	98.22	1.0853	1.0807	JRC ₃
JRC ₁₀	rbio 3.1	96.37	1.0800	1.0800	JRC ₁₀

4.3. Data Fusion and Decision-Making Process

Studies showed that different approaches lead to different results. In the stage of data fusion, in addition to studied methods, the results of the power spectrum (Table 4) (Sakellariou *et al* 1991), Box-Counting (Table 5) (Mohebbi *et al* 2015) and Hausdorff measurement (Table 6) (Martišek 2017) were considered (Figure 11). The ranking of the JRC profiles was achieved using the CSSD method. Also, the weighted directional graph is formed by using the decision matrix. In this matrix (Figure 12), features (f_i) are JRC profiles (JRC_i). After forming this weighted directional graph, one can consider the direction of edges as the increased roughness. In other words, the assigned values in each confrontation except from pairwise matrix arrays consider as the weight of edges. Therefore, we can consider their value as the weights of edges. These values are obtained from forming the pairwise matrix (Figure 12). Therefore, the vertices with the most output of edges have the least roughness. Also, the vertices that have the most input of edges are rougher and vice versa.

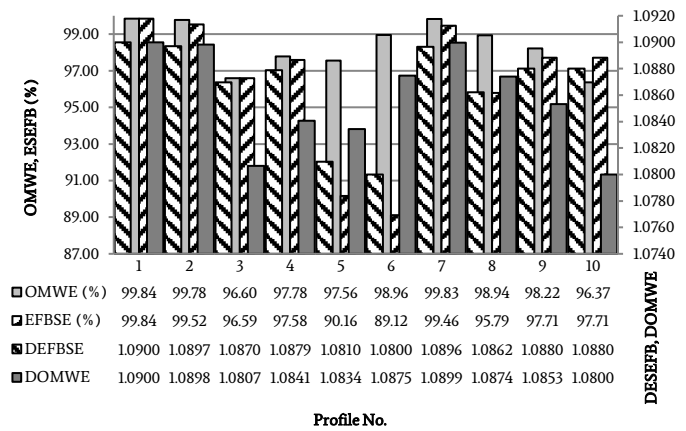


Figure 10. Optimum Mother Wavelet Energy in percent (OMWE), Effective Signal Energy of Frequency Band (ESEFB), obtained Dimension from Effective Frequency Band Signal Energy (DESEFB) and obtained Dimension from Optimum Mother Wavelet (DOMWE) versus JRC.

According to Figure 13, JRC₁ is the smoothest profile whereas JRC₁₀ is the roughest one. Due to the equality of inputs and outputs, re-ranking of profile 4, 5 and 6, were not straightforward. The ranking of other profiles are as follows:

$$\text{Increase roughness} = \{JRC_1, JRC_2, JRC_3, JRC_7, JRC_8, JRC_9, JRC_{10}\}$$

According to the weighted directional graph (Figure 14), the number of inputs and outputs for two profiles 6 and 4 are equal. On the other hand, the situation of profile 4 and 5 are ambiguous and this affects the position of profile 6. To overcome this ambiguity, the Borda Count method is used; because the inputs and outputs are similar for both and their weights are similar as well. For this purpose, the results of each method are written separately as follow in which each feature is written as F_{Number}^{Score} .

Table 4. The obtained results from regression between the normalized variance function and correlation length (Sakellariou *et al* 1991).

Range	Before Ranking		After Ranking	
	Original Ranking	Dimension	Dimension	New Ranking
0-2	JRC ₁	1.4930	1.1180	JRC ₈
2-4	JRC ₂	1.5190	1.1660	JRC ₆
4-6	JRC ₃	1.3600	1.1880	JRC ₁₀
6-8	JRC ₄	1.5220	1.2080	JRC ₇
8-10	JRC ₅	1.3470	1.2180	JRC ₉
10-12	JRC ₆	1.1660	1.3470	JRC ₅
12-14	JRC ₇	1.2080	1.3600	JRC ₃
14-16	JRC ₈	1.1180	1.4930	JRC ₁
16-18	JRC ₉	1.2180	1.5190	JRC ₂
18-20	JRC ₁₀	1.1880	1.5220	JRC ₄

Table 5. The obtained results from Box-Counting method (Mohebbi et al 2015).

Range	Before Ranking		After Ranking	
	Original Ranking	Dimension	Dimension	New Ranking
0-2	JRC ₁	1.1183	1.1183	JRC ₁
2-4	JRC ₂	1.1328	1.1328	JRC ₂
4-6	JRC ₃	1.1367	1.1358	JRC ₅
6-8	JRC ₄	1.1423	1.1367	JRC ₃
8-10	JRC ₅	1.1358	1.1423	JRC ₄
10-12	JRC ₆	1.1457	1.1457	JRC ₆
12-14	JRC ₇	1.1577	1.1577	JRC ₇
14-16	JRC ₈	1.1580	1.1580	JRC ₈
16-18	JRC ₉	1.1593	1.1593	JRC ₉
18-20	JRC ₁₀	1.1674	1.1674	JRC ₁₀

Table 6. The obtained results from Hausdorff measurement (Martišek 2017).

Range	Before Ranking		After Ranking	
	Original Ranking	Dimension	Dimension	New Ranking
0-2	JRC ₁	1.0230	1.0230	JRC ₁
2-4	JRC ₂	1.1470	1.1470	JRC ₂
4-6	JRC ₃	1.1920	1.1920	JRC ₃
6-8	JRC ₄	1.2410	1.2410	JRC ₄
8-10	JRC ₅	1.2860	1.2860	JRC ₅
10-12	JRC ₆	1.3140	1.3140	JRC ₆
12-14	JRC ₇	1.3350	1.3350	JRC ₇
14-16	JRC ₈	1.3570	1.3570	JRC ₈
16-18	JRC ₉	1.3650	1.3650	JRC ₉
18-20	JRC ₁₀	1.3980	1.3980	JRC ₁₀

$$Method_1 = \{JRC_{10}^1, JRC_3^9, JRC_5^8, JRC_6^7, JRC_4^6, JRC_8^5, JRC_9^4, JRC_1^3, JRC_2^2, JRC_{10}^1\}$$

$$Method_2 = \{JRC_{10}^1, JRC_3^9, JRC_5^8, JRC_6^7, JRC_4^6, JRC_5^5, JRC_7^4, JRC_3^3, JRC_8^2, JRC_{10}^1\}$$

$$Method_3 = \{JRC_{10}^1, JRC_3^9, JRC_5^8, JRC_6^7, JRC_4^6, JRC_5^5, JRC_9^4, JRC_3^3, JRC_7^2, JRC_{10}^1\}$$

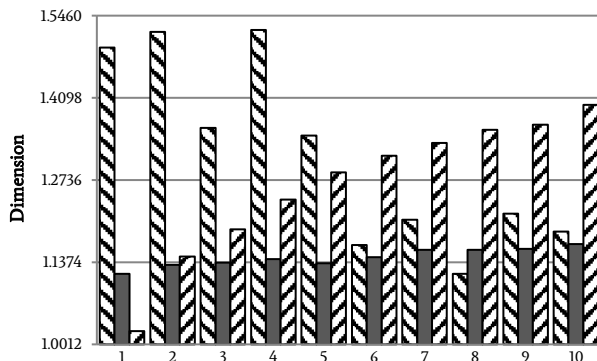
$$Method_{D_{ESEFB}} = \{JRC_{10}^1, JRC_3^9, JRC_2^8, JRC_7^7, JRC_{10}^6, JRC_4^5, JRC_3^4, JRC_8^3, JRC_5^2, JRC_6^1\}$$

$$Method_{D_{OMWE}} = \{JRC_{10}^1, JRC_3^9, JRC_2^8, JRC_6^7, JRC_8^6, JRC_9^5, JRC_4^4, JRC_5^3, JRC_3^2, JRC_{10}^1\}$$

$$Method_{Regression} = \{JRC_{10}^1, JRC_6^9, JRC_{10}^8, JRC_7^7, JRC_9^6, JRC_5^5, JRC_3^4, JRC_1^3, JRC_2^2, JRC_4^1\}$$

$$Method_{Box-Counting} = \{JRC_{10}^1, JRC_2^9, JRC_5^8, JRC_3^7, JRC_4^6, JRC_6^5, JRC_7^4, JRC_8^3, JRC_9^2, JRC_{10}^1\}$$

$$Method_{Hausdorff} = \{JRC_{10}^1, JRC_2^9, JRC_3^8, JRC_4^7, JRC_5^6, JRC_7^5, JRC_8^4, JRC_9^3, JRC_2^2, JRC_{10}^1\}$$



	Sakellariou et al. (1991)	Mohebbi et al. (2015)	Martišek (2017)
1	1.4930	1.1183	1.0230
2	1.5190	1.1328	1.1470
3	1.3600	1.1367	1.1920
4	1.5220	1.1423	1.2410
5	1.3470	1.1358	1.2860
6	1.1660	1.1457	1.3140
7	1.2080	1.1577	1.3350
8	1.1180	1.1580	1.3570
9	1.2180	1.1593	1.3650
10	1.1880	1.1674	1.3980

Profile No.

Figure 11. The obtained results from Sakellariou et al (1991), Mohebbi et al (2015) and Martišek (2017).

	JRC ₁	JRC ₂	JRC ₃	JRC ₄	JRC ₅	JRC ₆	JRC ₇	JRC ₈	JRC ₉	JRC ₁₀
JRC ₁	-	6	5	6	5	5	7	5	5	7
JRC ₂	2	-	7	8	7	7	6	7	7	7
JRC ₃	3	1	-	6	5	6	5	6	5	6
JRC ₄	2	0	2	-	4	3	5	6	5	6
JRC ₅	3	1	3	4	-	5	5	5	5	6
JRC ₆	3	1	2	5	3	-	6	6	7	7
JRC ₇	1	2	3	3	3	2	-	5	6	7
JRC ₈	3	1	2	2	3	2	3	-	6	7
JRC ₉	3	1	3	3	3	1	2	2	-	7
JRC ₁₀	1	1	2	2	2	1	1	1	1	-

Figure 12. Pairwise matrix using CSSD data fusion method for obtained result.

$$BC_{JRC_4} = \left(\begin{array}{c} \text{Higher priority} \\ \frac{JRC_1 \quad JRC_2 \quad JRC_3 \quad JRC_5 \quad JRC_6 \quad JRC_7 \quad JRC_8 \quad JRC_9 \quad JRC_{10}}{\tilde{2} + \tilde{0} + \tilde{2} + \tilde{4} + \tilde{3} + \tilde{5} + \tilde{6} + \tilde{5} + \tilde{6}} \\ \text{Lower priority} \\ \frac{JRC_1 \quad JRC_2 \quad JRC_3 \quad JRC_5 \quad JRC_6 \quad JRC_7 \quad JRC_8 \quad JRC_9 \quad JRC_{10}}{\tilde{6} + \tilde{8} + \tilde{6} + \tilde{4} + \tilde{5} + \tilde{3} + \tilde{2} + \tilde{3} + \tilde{2}} \end{array} \right) = 33 - 39 = -6$$

$$BC_{JRC_5} = \left(\begin{array}{c} \text{Higher priority} \\ \frac{JRC_1 \quad JRC_2 \quad JRC_3 \quad JRC_4 \quad JRC_6 \quad JRC_7 \quad JRC_8 \quad JRC_9 \quad JRC_{10}}{\tilde{3} + \tilde{1} + \tilde{3} + \tilde{4} + \tilde{5} + \tilde{5} + \tilde{5} + \tilde{5} + \tilde{6}} \\ \text{Lower priority} \\ \frac{JRC_1 \quad JRC_2 \quad JRC_3 \quad JRC_4 \quad JRC_6 \quad JRC_7 \quad JRC_8 \quad JRC_9 \quad JRC_{10}}{\tilde{5} + \tilde{7} + \tilde{5} + \tilde{4} + \tilde{3} + \tilde{3} + \tilde{3} + \tilde{3} + \tilde{2}} \end{array} \right) = 37 - 35 = 2$$

$$BC_{JRC_6} = \left(\begin{array}{c} \text{Higher priority} \\ \frac{JRC_1 \quad JRC_2 \quad JRC_3 \quad JRC_4 \quad JRC_5 \quad JRC_7 \quad JRC_8 \quad JRC_9 \quad JRC_{10}}{\tilde{3} + \tilde{1} + \tilde{2} + \tilde{5} + \tilde{3} + \tilde{6} + \tilde{6} + \tilde{7} + \tilde{7}} \\ \text{Lower priority} \\ \frac{JRC_1 \quad JRC_2 \quad JRC_3 \quad JRC_4 \quad JRC_5 \quad JRC_7 \quad JRC_8 \quad JRC_9 \quad JRC_{10}}{\tilde{5} + \tilde{7} + \tilde{6} + \tilde{3} + \tilde{5} + \tilde{2} + \tilde{2} + \tilde{1} + \tilde{1}} \end{array} \right) = 40 - 32 = 8$$

According to the obtained values, profile 6 is placed above two profiles 4 and 5. Therefore, the final ranking will be as presented in Table 7. The modified JRC (JRC_N) is presented in Figure 15. For making the final decision, the new status of profiles 4, 5 and 6 were compared to the original trend line (Figure 16). This comparison is based on the Taxicab norm (Equation 9) (Vetter 1970).

$$\|p - q\|_1 = \sum_{i=1}^n |p_i - q_i| \tag{9}$$

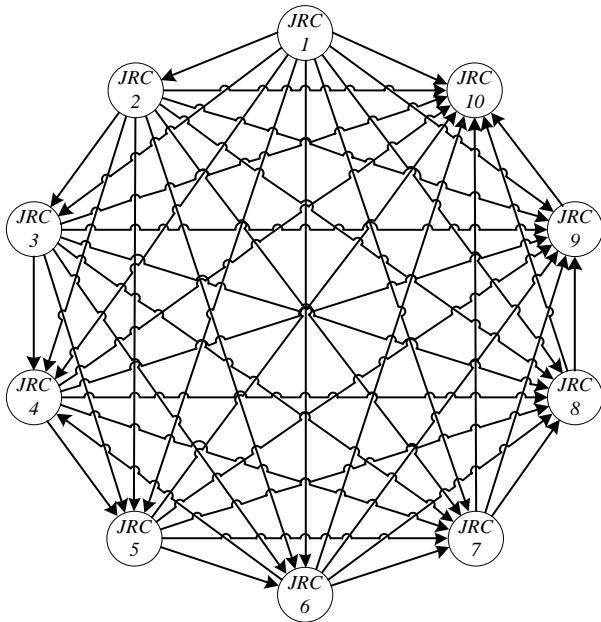


Figure 13. Framework of decision graph in CSSD method.

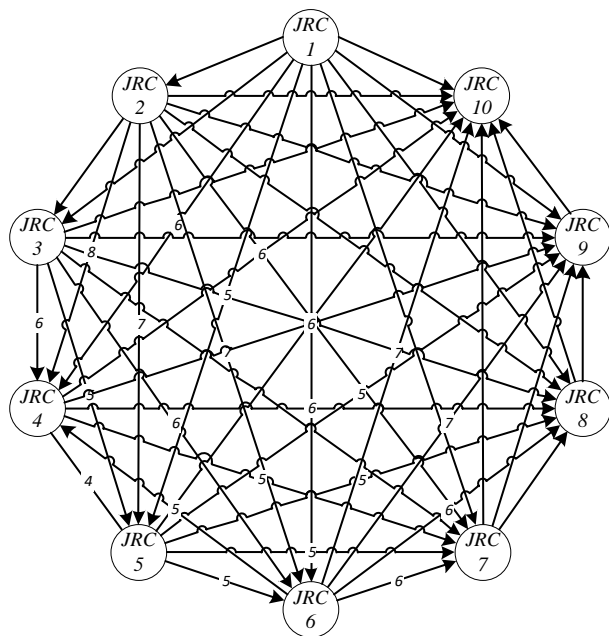
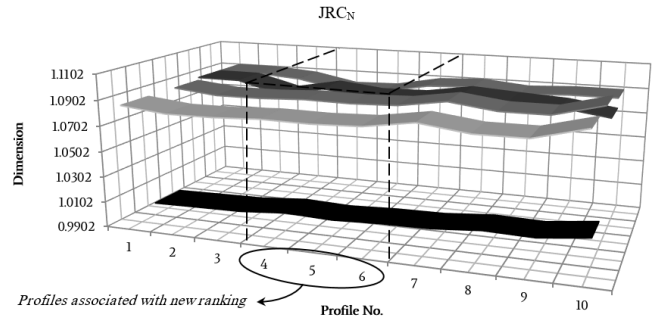


Figure 14. Weighted directional graph for decision making (Weights are written for three vertices 4, 5 and 6).

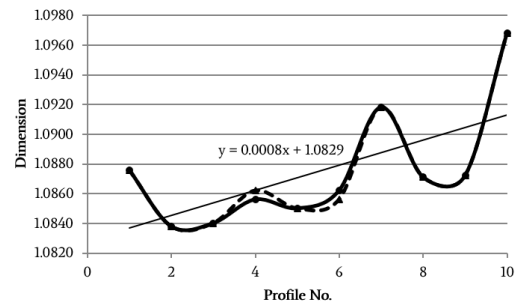
Table 7. Final rank of JRC exemplar profiles (JRC_N) using data fusion methods.

Before Sort	Range	Final Ranking After Measuring	JRC _N	Profile Number
JRC ₁	0-2	JRC ₁	JRC _{N1}	
JRC ₂	2-4	JRC ₂	JRC _{N2}	
JRC ₃	4-6	JRC ₃	JRC _{N3}	
JRC ₄	6-8	JRC ₆	JRC _{N4}	
JRC ₅	8-10	JRC ₅	JRC _{N5}	
JRC ₆	10-12	JRC ₄	JRC _{N6}	
JRC ₇	12-14	JRC ₇	JRC _{N7}	
JRC ₈	14-16	JRC ₈	JRC _{N8}	
JRC ₉	16-18	JRC ₉	JRC _{N9}	
JRC ₁₀	18-20	JRC ₁₀	JRC _{N10}	



	1	2	3	4	5	6	7	8	9	10
Method 1	1.0876	1.0838	1.0840	1.0856	1.0850	1.0862	1.0918	1.0871	1.0872	1.0968
Method 2	1.0001	1.0008	1.0014	1.0043	1.0029	1.0045	1.0050	1.0080	1.0071	1.0116
Method 3	1.0876	1.0838	1.0840	1.0856	1.0850	1.0862	1.0918	1.0871	1.0872	1.0968
DOMWE	1.0900	1.0898	1.0807	1.0875	1.0834	1.0841	1.0899	1.0874	1.0853	1.0800
DEFBSE	1.0900	1.0897	1.0870	1.0800	1.0810	1.0879	1.0896	1.0862	1.0880	1.0880

Figure 15. Ranking of JRC exemplar profiles after integration and turning it into the New JRC (JRC_N).



Error (JRC) 0.0041 Error (JRC_N) 0.0039

Method: Taxicab Norm

Figure 16. Comparing the error before (JRC) and after the ranking (JRC_N) - Dash line: Original Rank; Continuous line: New Rank.

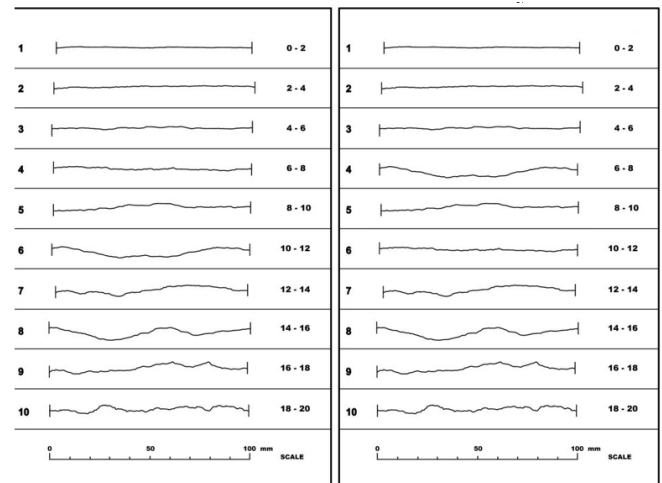


Figure 17. Roughness exemplar profiles – Original profiles (JRC) are in left and re-ranked profiles (JRC_N) applying data fusion method in right.

5. Conclusion

The CSSD and Borda Count approaches were used to the integration of different JRC ranking results. The results showed that the ranking of the majority of JRC's were remaining unchanged, whereas due to the ambiguity, an update is necessary for profiles 4, 5 and 6. In the modified JRC_N, profiles 6, 5, and 4 were ranked respectively. It confirmed that the newly ranked JRC is more robust in comparison with the common ranking. This result also is seen in the calculation of the error, before and after the ranking. It should be mentioned that in the current

research, the results of the JRC ranking of almost all published works were considered. Therefore, it might be claimed that the final ranking is the most robust one.

REFERENCES

- Amanloo F, Hosseinitoudeshki V (2013) The effect of joint roughness coefficient (JRC) and joint compressive strength (JCS) on the displacement of tunnel. *International Research Journal of Applied and Basic Sciences*, Science Explorer Publications. 4(8): 2216-2224.
- Arizabalo RD, Oleschko K, Korvin G, Ronquillo G, Cedillo-Pardo E (2004) Fractal and cumulative trace analysis of wire-line logs from a well in a naturally fractured limestone reservoir in the Gulf of Mexico. *Geofísica Internacional*. 43(3): 467-476.
- Asadi MS, Rasouli V, Tokhmechi B (2009) Wavelet analysis of JRC exemplar profiles. *Eurock 2009, Croatia: Balkema*, pp. 215-220.
- ASME (1978) American National Standard, Surface Texture, Surface Roughness, Waviness and Lay. American Society of Mechanical Engineers. New York.
- Babadagli T, Develi K (2001) On the application of methods used to calculate fractal dimension of fracture surfaces. *Fractals* 9(1): 105-128.
- Bae D, Kim K, Koh Y, Kim J (2011) Characterization of joint roughness in granite by applying the scan circle technique to images from a borehole televiewer. *Rock Mech. Rock Eng.* 44: 497-504.
- Barton N (1973) Review of a new shear strength criterion for rock joints. *Engineering Geology*. 7: 287-332.
- Barton N, Choubey V (1977) The shear strength of rock joints in theory and practice. *Rock Mechanics and Engineering Geology*. 10: 1-54.
- Barton CC, La Pointe PR (1995) *Fractals in petroleum geology and earth processes*: Plenum Press, New York.
- Brigham OE (1974) *The fast fourier transform*. Prentice-Hall, Inc. New Jersey, 133 p.
- Broumi S, Smarandache F (2013) Several similarity measures of neutrosophic sets. *Neutrosophic Sets Syst* 1(1):54-62.
- Brown SR (1987) A note on the description of surface roughness using fractal dimension. *Geophys. Res. Lett.* 14(11): 1095-1098.
- Bondy JA, Chvatal V (1976) A method in Graph Theory, *Discrete Mathematics*. 15: 111-135.
- Carpinteri A, Chiaia B (1995) Multifractal nature of concrete fracture surfaces and size effects on nominal fracture energy. *Mater Struc* 28:435-443.
- Cerepi A (2004) Geological control of electrical behaviour and prediction key of transport properties in sedimentary porous systems. *Colloids and Surfaces A: Physicochem. Eng. Aspects* 241: 281-298.
- Chae BG, Ichikawa Y, Jeong GC, Seo YS, Kim BC (2004) Roughness measurement of rock discontinuities using a confocal laser scanning microscope and the Fourier spectral analysis. *Engineering Geology* 72: 181-199.
- Chun BS, Kim DY (2001) A numerical study on the quantification of rock joint roughness. *J KGS* 17:88-97.
- Cox BL, Wang JSY (1993) Fractal surfaces: measurement and applications in the earth sciences. *Fractals* 1:87-115.
- Den Outer A, Kasshoek JF, Hack HRGK (1995) Difficulties with using continuous fractal theory for discontinuity surfaces. *Int. J. Rock Mech. Min. Sci. Geomech. Abstr.* 32(1): 3-9.
- Develi, K., (1996), The quantitative definition of joint surface roughness of Kurtun Dam site rocks in Harsit Valley, Turkey: unpubl. MS thesis, Istanbul Technical University, Istanbul, Turkey, 150 p.
- Du S, Gao H, Hu Y, Huang M, Zhao H (2015) A New Method for Determination of Joint Roughness Coefficient of Rock Joints. *Mathematical Problems in Engineering*, Article ID 634573, p. 6.
- Dubuc B, Quiniou JF, Roques-Carmes C, Tricot C, Zucker SW (1989) Evaluating the fractal dimension of profiles. *Phys. Rev. A* 39(3): 1500-1512.
- Feder J (1988) *Fractals*. Plenum Press, New York, p.238.
- Ferrero M, Iabichino G, Pancotti G, Giani GP (1999) Interpretazione con modelli matematica di misure di rugosità di discontinuità naturali in roccia XX convegno nazionale di geotecnica: 101-106 (in Italian).
- Fishburn PC (1984) *Discrete Mathematics in Voting and Group Choice*. 5(2): 263-275.
- Ghazvinian A, Mohebi M (2012) Investigation and correcting factors offering for roughness corresponding to Barton Standard classes with quantitative fractal techniques. 4th Conference on Mining Engineering. University of Tehran. Iran, pp. 55-61 (in Persian).
- Glover PWJ, Matsuki K, Hikima R, Hayashi K (1999) Characterizing rock fractures using synthetic fractal analogues. *Geotherm. Sci. & Tech.* 6: 83-112.
- Grzeski W, Brol S (2009) Wavelet and fractal approach to surface roughness characterization after finish turning of different workpiece materials. *Journal of Materials Processing Technology*. 209: 2522-2531.
- Halling J (1976) *Introduction to Tribology*, Wykeham, London.
- Hudson JA, Harrison JP (1997) *Engineering Rock Mechanics An Introduction to the Principles*, p. 456, ISBN: 9780080530963.
- Harary F (1969) *Graph Theory*, Addison-Wesley, Reading, Massachusetts, p. 206.
- Huai SU, Enrico Z, Jinjun ZH, Xueyi L (2018) A Systematic Framework of Vulnerability Analysis of a Natural Gas Pipeline Network, *Reliability Engineering and System Safety*.
- Hung Yau Y (1978) *Displacement and strain measurement*. Speckle Metrology. Academic Press, New York, 51-72.
- Huang SL, Oelfke SM, Speck RC (1992) Applicability of fractal characterization and modeling to joint profiles. *Int. J. Rock Mech. Min. Sci. Geomech. Abstr.* 29(2): 89-98.
- Huang X, Zhu J, Li J, Bai B, Zhang G (2016) Fluid friction and heat transfer through a single rough fracture in granitic rock under confining pressure, *International Communications in Heat and Mass Transfer* 75: 78-85.
- Jain R, Pitchumani R (2017) *Fractal Model for Wettability of Rough Surfaces*. American Chemical Society Publications, Langmuir, 33: 7181-7190.
- Josso B (2000) New wavelet-based space-frequency analysis methods applied to the characterisation of three-dimensional engineering surface textures. Ph.D. Thesis. Liverpool John Moores University.
- Josso B, Burton DR, Lator MJ (2001) Wavelet strategy for surface roughness analysis and characterization. *Comput. Methods Appl. Mech. Eng.* 191(8-10): 829-842.
- Josso B, Burton DR, Lator MJ (2002) Frequency normalized wavelet transform for surface roughness analysis and characterization. *Wear*. 252: 491-500.
- Khakzad N, Reniers G (2015) Using Graph Theory to Analyze the Vulnerability of Process Plants in the Context of Cascading Effects, *Reliab. Eng. Syst. Saf.* 143: 63-73.

- Kulatilake P, Shou G, Huang TH, Morgan RM (1995) New peak shear strength criteria for anisotropic rock joints. *Int J Rock Mech Min Sci* 32:673–697.
- Kulatilake P, Um J, Pan G (1998) Requirements for accurate quantification of self-affine roughness using the variogram method. *Int J Solids Struct*, 35(31):4167–89.
- Lee SH, Zahouani H, Carenti R, Mathia TG (1998) Morphological characterization of engineered surfaces by wavelet transform. *Int. J. Mach. Tools Manuf.* (28): 581–589.
- Lee YH, Carr JR, Barr DJ, Haas CJ (1990) The Fractal Dimension as a Measure of the Roughness of Rock Discontinuity Profiles. *Int. J. Rock Mech. Min. Sci. & Geomech. Abstr.* 27(6): 453–464.
- Li Y, Huang R (2015) Relationship between joint roughness coefficient and fractal dimension of rock fracture surfaces. *International Journal of Rock Mechanics & Mining Sciences*. 75: 15–22.
- Maerz NH, Franklin JA, Bennett CP (1990) Joint roughness measurement using shadow profilometry. *Int. J. Rock Mech. Min. Sci. Geomech. Abstr.* (27): 329–343.
- Majumdar P, Samanta SK (2014) On similarity and entropy of neutrosophic sets. *J Intell Fuzzy Syst* 26(3):1245–1252.
- Martišek D (2017) Joint Rock Coefficient Estimation Based on Hausdorff Dimension, *Advances in Pure Mathematics*, 7, 615–640.
- McWilliams PC, Kerker JC, Miller SM (1993) Estimation of Shear Strength Using Fractals as a Measure of Rock Fracture Roughness, Report of Investigations 9447, UNITED STATES DEPARTMENT OF THE INTERIOR.
- Miller SM, McWilliams PC, Kerker JC (1990) Ambiguities in estimating fractal dimensions of rock fracture surfaces. *Hustrulid, W., Johnson, G.A., Rock Mech. Contribution Challenges*. Balkema, Rotterdam. pp. 471–478.
- Mohebbi M., Yarahmadi Bafghi A., Fatehi Marji M., Gholamnejad J (2015) Accurate Estimation of Scale Independent Joint Roughness Coefficient, JRC, by Optimized Box-Counting Algorithm, *Indian Journal of Fundamental and Applied Life Sciences*, Vol. 5 (S3), pp. 2427-2442.
- Mooney CR, Boisvert JB (2015) Using a Discrete Fracture Network and Spatial Point Processes to Populate Veins and Model Grade in a Coarse Gold Deposit. *International Association for Mathematical Geosciences*, doi: 10.1007/s11053-015-9280-1.
- Moosavi M, Rafsanjani HN, Mehranpour MH, Nazem A, Shirazi AN (2013) An investigation of surface roughness measurement in rock joints with a 3D scanning device. The 3rd International Society for Rock Mechanics on “Rock Characterisation, Modelling and Engineering Design Methods”, Tongji University, Shanghai, China.
- Morala-Argüello P, Barreiro J, Alegre E (2012) A evaluation of surface roughness classes by computer vision using wavelet transform in the frequency domain. *Int. J. Adv. Manuf. Technol.* 59(1–4): 213–220.
- Moslehian MS, Amer Payhan MS (2005) *How Is the Winner?* Thehran, Sokhan Gostar Publisher (in Persian).
- Murata S, Mitsuishi H, Saito T (2002) Characterization of fracture permeability by using a fractal model. SPE 77881. *Proceedings of the Asia Pacific oil and Gas Conference and Exhibition*. Melbourne, Australia, 8–10: 1–8.
- Moulin H (1988) *Axioms of co-operative decision making*. Econometric Society Monographs. Cambridge University Press. Cambridge.
- Nayak SR, Mishra J (2016) An Improved Method to Estimate the Fractal Dimension of Color Images. *Perspectives in Science*, <http://dx.doi.org/10.1016/j.pisc.2016.04.092>.
- Newenhizen JV (1992) The Borda Method is most likely to Respect the Condorcet Principle. *Econ. Theory*, 2: 69–83.
- Olsen WS, Adams RM (1970) A laser profilometer, *J. Geophys. Res.* 75: 2185–2187.
- Orey S, (1970) Gaussian sample functions and the Hausdorff dimension of level crossings. *Probability Theory and Related Fields.* (15)3: 249–256.
- Osterloo MM, Hamilton VE, Anderson FS (2012) A laboratory study of the effects of roughness on the thermal infrared spectra of rock surfaces. *Icarus* 220: 404–426.
- Panigrahy C, Garcia-Pedrero A, Seal A, Rodríguez-Esparragón D, Kumar Mahato N, Gonzalo-Martín C (2017) An Approximated Box Height for Differential-Box-Counting Method to Estimate Fractal Dimensions of Gray-Scale Images. *Entropy*, 19, 534; doi:10.3390/e19100534.
- Press WH, Teukolsky SA, Vetterling WT, Flannery BP (1992) *Numerical recipes in C: The art of scientific computing*. Cambridge University Press, USA, p. 504.
- Rasouli V, Tokhmechi B (2010) Difficulties in Using Geostatistical Models in Reservoir Simulation. *SPE* 126191, Egypt.
- Roko RO, Daemen JJK, Myers DE (1997) Variogram characterization of joint morphology and asperity deformation during shearing. *International Journal of Rock Mechanics and Mining Sciences and Geomechanics Abstracts*, 34: 71–84.
- Sakellariou M, Nakos B, Mitsakaki C (1991) On the fractal character of rock surfaces. *Int J Rock Mech Min Sci Geomech Abstr*; 28:527–33.
- Saupe D (1988) Algorithms for random fractals, in: Saupe, D., Peitgen, H.O., eds., *The science of fractal image*: Springer-Verlag, New York, pp. 71–113.
- Seidel JP, Haberfield CM (1995) Towards an understanding of joint roughness. *Rock Mech Rock Eng* 28:69–92.
- Seno T (2003) Fractal asperities, invasion of barriers, and interplate earthquakes. *Earth Planets Space*, 55: 649–665.
- Shah J (2009) *Hausdorff Dimension and Its Application*. SiteSeerx. The College of Information Sciences and Technology. 10 pages. <http://citeseerx.ist.psu.edu/viewdoc/citations?doi=10.1.1.642.6826>.
- Shou G (1994) *Joint Roughness Characterization and Effect of Roughness on Peak Shear Strength of Joints*. PhD Thesis, DEPARTMENT OF MINING AND GEOLOGICAL ENGINEERING, THE UNIVERSITY OF ARIZONA.
- Suleimanov AB, Guseynova NI, Veliyev EF (2017) Control of Displacement Front Uniformity by Fractal Dimensions, *SPE-187784-MS*.
- Tatone BSA (2009) Quantitative characterization of natural rock discontinuity roughness in-situ and in the laboratory. Ph.D. thesis, University of Toronto, Toronto, Canada.
- Tatone BSA, Grasselli G (2010) A new 2D discontinuity roughness parameter and its correlation with JRC. *International Journal of Rock Mechanics & Mining Sciences*. 47: 1391–1400.
- Tatone BSA, Grasselli G (2013) An investigation of discontinuity roughness scale dependency using high-resolution surface measurements. *Rock Mechanics and Rock Engineering*, 46(4): 657–681.
- Thachaparambil MV (2015) Discrete 3D fracture network extraction and characterization from 3D seismic data — A case study at Teapot Dome. SEG.
- Thomas TR (1982) *Rough Surfaces*. Longman, London.
- Tokhmechi B, Lotfi M, Seifi H, Hosseini MS (2016) *Data Fusion, A New Approach for Decision Making in Geology, Mining and Petroleum Engineering*, Amirkabir University of Technology (Tehran Polytechnic) Press, Tehran, p. 808, ISBN: 978-964-463-656-1 (in Persian).

- Tran NH, Tran K (2007) Combination of fuzzy ranking and simulated annealing to improve discrete fracture inversion. *Mathematical and Computer Modelling*, 45: 1010–1020.
- Tse R, Cruden D (1979) Estimating joint roughness coefficients. *International Journal of Rock Mechanics and Mining Sciences & Geomechanics*. 16: 303–307.
- Tzschichholz F, Herrmann HJ (1995) Simulations of pressure fluctuations and acoustic emission in hydraulic fracturing. *Phys. Rev. E* 51: 1961–1970.
- Unal M (2000) Modelling of discontinuity surface roughness and investigation of its effects on shear strength. PhD thesis, Hacettepe University, Ankara, p. 219.
- Um JG (1997) Accurate quantification of rock joint roughness and development of a new peak shear strength criterion for joints. PhD Thesis, DEPARTMENT OF MINING AND GEOLOGICAL ENGINEERING, THE UNIVERSITY OF ARIZONA.
- Wu D, Mendel JM (2008) A vector similarity measure for linguistic approximation: interval type-2 and type-1 fuzzy sets. *Inform Sci* 178(2):381–402.
- Xie H, Wang JA, Xie WH (1997) Fractal Effect of Surface Roughness on the Mechanical Behavior of Rock Joints. *Chaos, Solitons & Fractals*, 8(2): 221–252.
- Yang ZY, Di CC, Yen KC (2001) The effect of asperity order on the roughness of rock joints. *International Journal of Rock Mechanics and Mining Sciences*, 38(5): 745–752.
- Ye J (2011) Cosine similarity measures for intuitionistic fuzzy sets and their applications. *Math Comput Model* 53(1):91–97.
- Ye J (2012) Multicriteria decision-making method using the Dice similarity measure based on the reduct intuitionistic fuzzy sets of interval-valued intuitionistic fuzzy sets. *Appl Math Model* 36(9):4466–4472.
- Ye J (2014) Vector similarity measures of hesitant fuzzy sets and their multiple attribute decision making. *Econ Comput Econ Cybern Stud Res* 48(4).
- Ye J (2015) Improved cosine similarity measures of simplified neutrosophic sets for medical diagnoses. *Artif Intell Med* 63:171–179.
- Yong R, Fu X, Huang M, Liang Q, Du SG (2018) A Rapid Field Measurement Method for the Determination of Joint Roughness Coefficient of Large Rock Joint Surfaces. *KSCE Journal of Civil Engineering* 22(1): 101–109.
- Yu X, Vayssade B (1991) Joint profiles and their roughness parameters. *International Journal of Rock Mechanics and Mining Sciences & Geomechanics Abstracts*, 28(4): 333–336.
- Zhang G, Karakus M, Tang H, Ge Y, Zhang L (2014) A new method estimating the 2D Joint Roughness Coefficient for discontinuity surfaces in rock masses. *International Journal of Rock Mechanics & Mining Sciences* 72: 191–198.
- Zuo X, Zhu H, Zhou Y, Yang J (2017) Estimation of fractal dimension and surface roughness based on material characteristics and cutting conditions in the end milling of carbon steels. *Journal of Engineering Manufacture*, 231(8): 1423–1437.